Journal of Materials Chemistry A

Accepted Manuscript

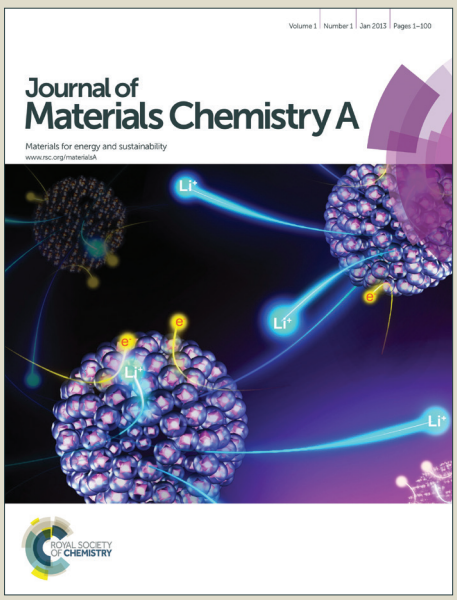

ROYAL SOCIETY OF CHEMISTRY

www.rsc.org/materialsA

PO_4^{3-} polyanion-doping for stabilizing Li-rich layered oxides as cathode for advanced lithium-ion batteries

H. Z. Zhang, Q. Q. Qiao, G. R. Li, X. P. Gao

TOC

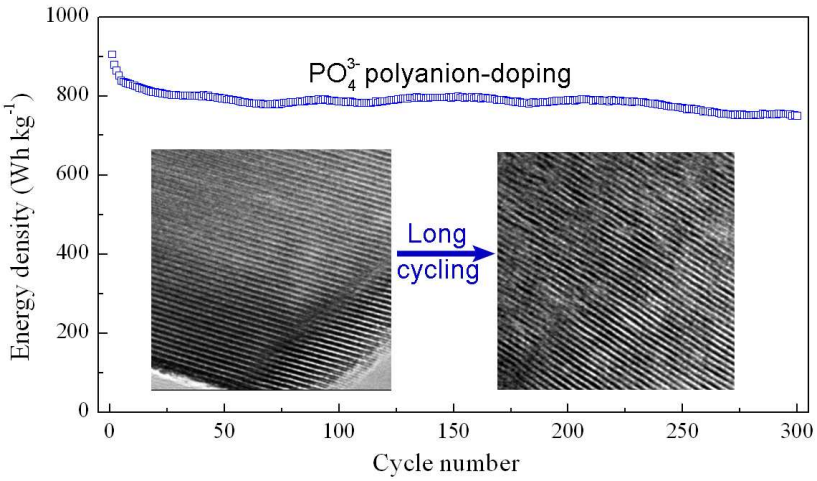

PO_4^{3-} polyanion-doped Li-rich layered oxides offer excellent energy density retention during long cycling due to the stronger anion bonding of PO_4^{3-} polyanions to transition metal cations.

Journal of Materials Chemistry A

Cite this: DOI: 10.1039/c0xx00000x

Paper

www.rsc.org/xxxxxx

PO_4^{3-} polyanion-doping for stabilizing Li-rich layered oxides as cathode for advanced lithium-ion batteries

H. Z. Zhang, Q. Q. Qiao, G. R. Li, and X. P. Gao*

Received (in XXX, XXX) Xth XXXXXXXXX 20XX, Accepted Xth XXXXXXXXX 20XX

DOI: 10.1039/b000000x

Advanced Li-ion batteries with Li-rich layered oxides as cathode and Si-based composites as anode, are considered as high energy battery systems for the next generation of smart communications and electric vehicles (EVs). At current stage, it is significant to develop Li-rich layered oxides with stable output energy density. However, the gradual capacity degradation and potential decay during cycling lead to the continual decrease in the energy density of Li-rich layered oxides. Therefore, new strategy should be introduced to block the migration of transition metal cations and maintain the parent layered structure during cycling, in order to stabilize the energy density of oxides. In this work, large tetrahedral PO_4^{3-} polyanions with high electronegativity in respect to O^{2-} anions are doped into the oxide for minimizing the local structure change during cycling. When doping with PO_4^{3-} polyanions, the parent layered structure retains during long cycling, due to the strong bonding of PO_4^{3-} polyanions to transition metal cations (Ni especially). Correspondingly, PO_4^{3-} polyanion-doped oxides present excellent energy density retention during long cycling, integrated with discharge capacity and midpoint potential. These results suggest that polyanion-doping can meet the performance requirement of stabilizing the energy density of Li-rich layered oxides for advanced lithium ion batteries.

1. Introduction

High energy density is of primary concern for Li-ion batteries in the practical application of smart communications and electric vehicles (EVs).[1-3] To fabricate advanced Li-ion batteries, it is highly significant to explore and develop new cathode materials with large specific capacity, the capacity-determining electrode and the source of lithium in Li-ion battery systems. In recent years, Li-rich layered oxides with an anomalously large specific capacity of over 250 mAh g^{-1},[4-14] have been extensively investigated as cathode materials for advanced Li-ion batteries, coupled with Si-based anode materials. Although the electrochemical reaction mechanisms proposed previously are still under debate, the large capacity of Li-rich layered oxides is truly obtained, which is usually explained as the nickel (Ni^{2+}/Ni^{4+}) and manganese (Mn^{3+}/Mn^{4+}) valence variation, associated with anion redox reaction (O^{2-}/O_2^{2-}).[11] Undoubtedly, both the large specific capacity and long cycle stability are indispensable for Li-rich layered oxides, offering a potential possibility to meet the demands on high energy Li-ion batteries. It is also important to note that the discharge capacity stability and discharge potential stability in the electrochemical reaction process should be simultaneously achieved in order to maintain high energy density of the cathode. However, these Li-rich layered oxides exhibit a gradual discharge potential plateau drop during cycling,[14-15] leading to the continual decrease in the energy density of the cathode, although good discharge capacity retention can still be achieved.

At present, considerable attention has been paid to the surface modification with metal oxides,[12,16-17] fluorides,[14,18-20] and phosphates,[16, 21-22] for improving the discharge capacity stability of Li-rich layered oxides. Indeed, the discharge capacity stability of Li-rich layered oxides is greatly improved by the surface modification, which can slow down the formation of spinel phase initiated from the particle surface.[14-15] However, the requirement for the discharge potential plateau stability during cycling is still unsatisfied in such surface modified Li-rich layered oxides due to the gradual local structure change from the layered structure to the cubic spinel in the bulk phase.[14-15] It should be mentioned that the discharge potential plateau of the cathode is highly related to the stability of the crystallographic structure, which could be improved by stronger anion bonding to transitional metal cations in Li-rich layered oxides. Specifically, large tetrahedral PO_4^{3-} polyanions with high electronegativity in respect to spherical O^{2-} anions can be doped into Li-rich layered oxides, which may stabilize the local structure for achieving the stable energy density of the cathode.

In this work, we propose a proof-of-concept of fixing transition metal cations in the layered structure by large tetrahedral PO_4^{3-} polyanions and stabilizing energy density of Li-rich layered $Li(Li_{0.17}Ni_{0.20}Co_{0.05}Mn_{0.58})O_2$ (LNCMO) oxides

during cycling. After introducing an optimized amount of PO_4^{3-} polyanions, the local environment in the layered structure would be changed to a certain extent due to the synergistic function of PO_4^{3-} polyanions with O^{2-} anions in the oxide. The feasibility of stabilizing the energy density for the PO_4^{3-} polyanion-doped Li-rich layered oxides during long cycling is firstly explored.

2. Experimental

Preparation and characterization.

All the samples were prepared by the combination of spray-drying and solid-state reaction. The manganese, nickel and cobalt acetate tetrahydrates (analytical grade) with the stoichiometric amount, and lithium acetate dihydrate (analytical grade) with 5% excessive amount (mole ratio) were dissolved in distilled water to obtain the mixed solution. The concentration of the metal ions was 0.5 mol L^{-1}. After then, the solution was dripped slowly into the mixed solution of citric acid monohydrate (analytical grade, $C_6H_8O_7•H_2O$) and ammonium phosphate (analytical grade, $NH_4H_2PO_4$) with vigorous stirring. The molar ratio of citric acid to metal ion was 2:1, and metal ion concentration in the final solution was 0.2 mol L^{-1}. The pH value of the solution was controlled at 9, which was adjusted by ammonia solution (25 wt %). The resulting solution was pumped into a spray drying instrument (L217, LaiHeng) to produce a homogenous precursor. The precursor was initially decomposed at 480 °C for 5 h in air. After being ground, the resulting powder was put into a corundum crucible and calcined at 850 °C for 10 h, and then quenched in water to obtain the sample. According to the different molar concentration of PO_4^{3-} polyanoins, four samples were marked as LNCMO, LNCMO-$(PO_4)_{001}$, LNCMO-$(PO_4)_{003}$ and LNCMO-$(PO_4)_{005}$, respectively. The structure, morphology and surface state of the samples were detected using X-ray diffraction (XRD, Rigaku D/MAX-2500v/pc), scanning electron microscopy (SEM, Hitachi S-4800), transmission electron microscopy (TEM, FEI Tecnai F20), Fourier transform infrared spectra (FTIR, Bruker Tensor 27), and X-ray photoelectron spectroscopy (XPS, PHI5000 VersaProbe). Reitveld refinement was applied for data analysis using the WinplotR package.[23]

Electrochemical measurement.

The obtained sample, acetylene black, and polytetrafluoroethylene (PTFE, as binder) were mixed at a weight ratio of 75:15:10, and compressed to prepare the working electrode. A metallic lithium foil was used as the counter and reference electrodes. The electrolyte was $LiPF_6$ (1M) in a mixture of ethylene carbonate (EC) and dimethyl carbonate (DMC) with a volume ratio of 3:7. The galvanostatic charge and discharge tests were performed between 2.0 and 4.8 V (vs Li/Li^+) with LAND CT-2001A instrument (Wuhan, China) at RT. Electrochemical impedance spectra (EIS) were measured using a Zahner IM6ex electrochemical workstation in the frequency range of 100 kHz to 10 mHz.

3. Results and discussion

As shown in **Fig. 1a**, all the diffraction peaks of the PO_4^{3-}-doped oxides can be indexed as the O3 type layered structure (space group $R\bar{3}m$). The additional weak reflections of the short-ranged superstructure around 2θ = 20–22° are attributed to the existence of the Li_2MnO_3-like component with the monoclinic structure (space group C2/m), as well as the ordering of Li, Ni, Co, and Mn cations in the transition metal layers.[6,17,24-25] There are no impurities of olive phosphates, implying that the PO_4^{3-} polyanions can be almost doped into the crystallographic structure of the oxide. In particular, the superstructure of the Li_2MnO_3-like component is more obvious with higher PO_4^{3-} polyanion concentration (PO_4^{3-}=0.05) as shown in **Fig. 1b**. As more PO_4^{3-} polyanions are added (PO_4^{3-}=0.07), the strong Li_2MnO_3-like component can be detected with an uncertain phase and an impurity species (Li_3PO_4), resulting in lower capacity (**Fig. S1**). In addition, with increasing the PO_4^{3-} polyanion concentration, the c-lattice parameter and c/a ratio increase (**Table 1**), implying the slight expansion of the Li layer in the layered structure on account of the large tetrahedral PO_4^{3-} polyanions (thermochemical radii 238 pm) in respect to spherical O^{2-} anions (ionic radii 140 nm).[26] The analogous expansion of the layered structure is also demonstrated in Li-rich layered oxides with doping of large cations, such as Na^+ ions or Y^{3+} ions,[27-28] which could be ascribed to a pillar effect. Generally, the $I_{(003)}/I_{(104)}$ intensity ratio can be used to characterize the degree of cation mixing in the Li-layers.[12,29] The $I_{(003)}/I_{(104)}$ intensity ratio in the as-prepared oxide is 1.085, implying relatively larger degree of cation mixing. After introducing PO_4^{3-} polyanions, the $I_{(003)}/I_{(104)}$ intensity ratio dramatically increases (>1.23), demonstrating the lower cation mixing in the PO_4^{3-}-doped oxides, which is favorable for improving the electrochemical cycle stability. The morphology and grain size of the PO_4^{3-}-doped samples are almost identical to the as-prepared oxide (**Fig. S2**).

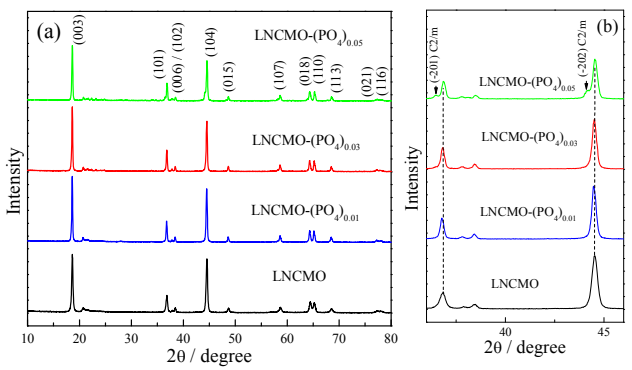

Fig. 1 Structure characterization of the oxides. (a) Full XRD patterns, (b) Local magnified XRD patterns near (101) and (104) peaks.

Table 1 The crystallographic parameters of the samples.

Sample	a / Å	c / Å	c/a	$I_{(003)}/I_{(104)}$
LNCMO	2.8602	14.2101	4.968	1.085
LNCMO-$(PO_4)_{0.01}$	2.8614	14.2652	4.985	1.230
LNCMO-$(PO_4)_{0.03}$	2.8589	14.2686	4.991	1.285
LNCMO-$(PO_4)_{0.05}$	2.8565	14.2687	4.995	1.373

To identify the presence of the PO_4^{3-} polyanions, FTIR spectra are conducted and shown in **Fig. 2**. The characteristic peaks at about 550 and 624 cm^{-1} are observed in all the samples,

which are assigned to the asymmetric stretching modes of M-O bonds in MO_6 octahedra and the O-M-O bending modes.[30] The doping of the PO_4^{3-} polyanions weakens the M-O bonding due to the stronger interaction of adjacent PO_4^{3-} polyanions, Accordingly, the peak at 550 cm^{-1} shifts to lower wavenumbers (542, 537, and 529 cm^{-1}). Meanwhile, the bands at 1039 and 1096 cm^{-1} appear in the PO_4^{3-}-doped samples, attributed to the asymmetric stretching P–O vibrations in PO_4^{3-} ions.[31]

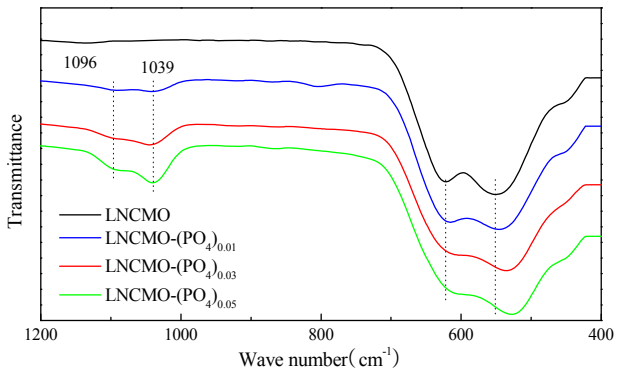

Fig. 2 FTIR spectra of the oxides.

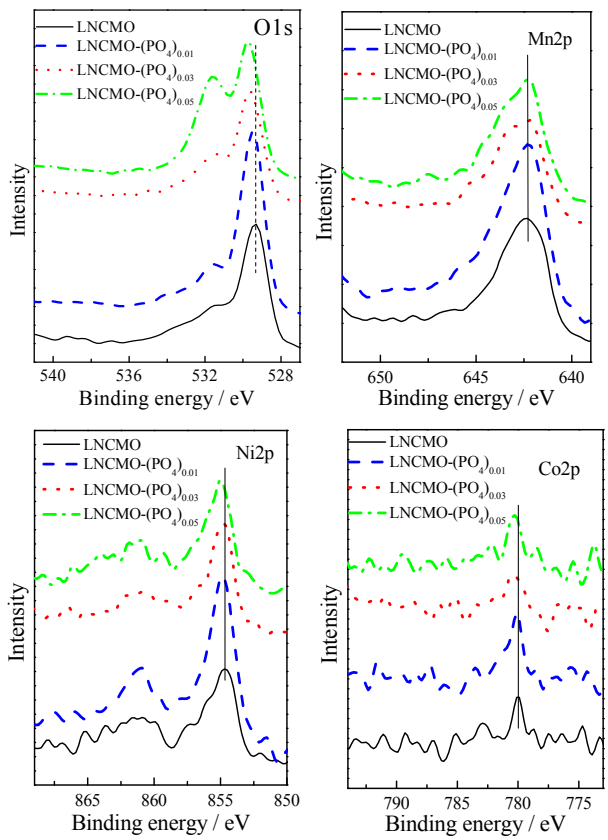

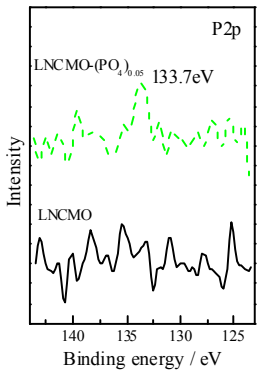

Fig. 3 XPS spectra of the oxides (O1s, Mn2p, Ni2p, Co2p and P2p core levels).

The bonding interaction is further verified by XPS (**Fig. 3**). The O1s core levels show a slight change between the as-prepared and PO_4^{3-}-doped samples. There is a strong O1s peak at 529.3 eV, corresponding to the lattice oxygen of the Li-rich layered oxides,[17] which gradually shifts to higher binding energy (529.5, 529.6, and 529.8 eV) in the PO_4^{3-}-doped samples due to the strong electron interaction of PO_4^{3-} polyanions with high electronegativity. Besides, the peak at 531.6 eV is stronger with increasing the PO_4^{3-} concentration, which is consistent with that of PO_4^{3-}.[32] The center of P2p peak of the LNCMO-$(PO_4)_{005}$ sample is located at 133.7 eV, which is attributed to the presence of phosphate groups in transition metal phosphates.[22,33-34] Correspondingly, the peaks of $Ni2p_{3/2}$ and $Co2p_{3/2}$ are measurably moved to higher binding energy with increasing PO_4^{3-} concentration, ascribed to the local environment change originated from the introduction of PO_4^{3-} polyanions with higher electronegativity with respect to O^{2-} anions.[35] In addition, the charge compensation is accomplished by the slightly change of binding energy of Ni/Co cations, as O^{2-} anions are partially replaced by PO_4^{3-} polyanions in the doped-oxides. The binding energy of $Mn2p_{3/2}$ is located at 642.3 eV for all the samples, in accordance with the Mn^{4+} valence state in Li-rich layered oxides. It means that the bonding of Ni/Co cations to anions is enhanced with doping PO_4^{3-} polyanions, while the oxidation state of Mn cations is maintained unchanged regardless of PO_4^{3-}-doping. Therefore, PO_4^{3-} polyanion-doping only alters the local environment of the Li-rich layered oxides moderately.

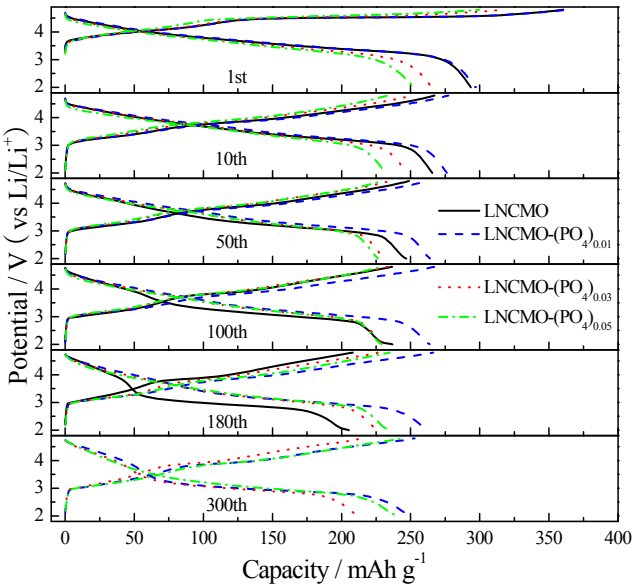

Fig. 4 The charge–discharge curves of the oxides in different cycles at 0.1C rate (30 mA g^{-1}) between 2.0 and 4.8 V (vs Li/Li^+) at RT.

Fig. 4 shows the charge-discharge curves of all the samples during cycling at 0.1 C rate. In the initial cycle, the discharge capacity of the as-prepared sample is 293.5 mAh g^{-1}, while the discharge capacities are 296.7, 265.2, and 252.4 mAh g^{-1} with increasing PO_4^{3-} polyanion concentration in the oxide. The initial coulombic efficiency increases slowly from 81.4 % for the as-prepared sample to 81.5, 83.4, and 84.2 % for the PO_4^{3-}-doped samples. In addition, good rate capability is still obtained for the PO_4^{3-}-doped samples, as shown in **Fig. 5**, which is in consistent with the change of the charge-transfer resistance and diffusion impedance within the initial cycles (**Fig. S3 and S4**).

During long cycling, the discharge capacity degradation of the as-prepared sample is serious, accompanied with notable increase of the electrochemical impedance, including the charge-transfer resistance and diffusion impedance (**Fig. S4**). In particular, in the 100th and 180th cycles, the sloped discharge curve splits into two plateaus of high and low potential (around 4.0 and 3.0 V vs. Li/Li^+), implying the local structure transition from hexagonal structure to cubic spinel.[14-15,36-38] After 300 cycles, the discharge potential decay is still observed for all the PO_4^{3-}-doped samples, which is mainly ascribed to the gradual local structure change. In particular, the plateau split into high and low potentials appears for the Li-rich layered oxide with a low PO_4^{3-} polyanion concentration (for example for PO_4^{3-}=0.01) in the 300th cycle. This finding reveals that PO_4^{3-} polyanions with low concentration in the Li-rich layered oxide can slow down, instead of terminate, the local structure transition from layered structure to layered/spinel coexistence during long cycling.

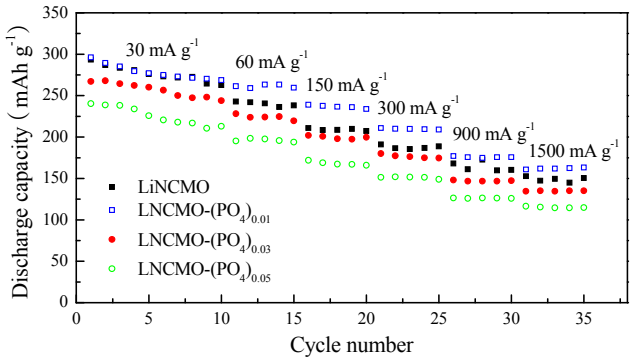

Fig. 5 The rate performance of the oxides between 2.0 and 4.8 V (vs Li/Li^+) at RT.

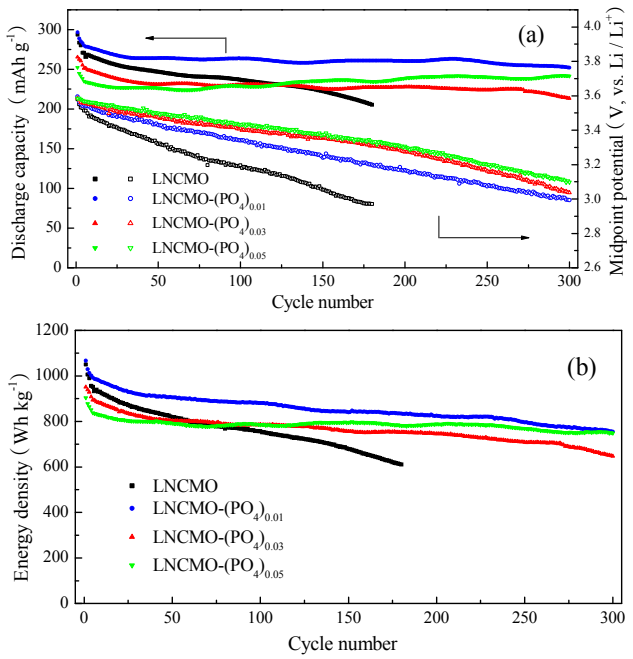

Fig. 6 The cycle performance of the oxides at 0.1C rate between 2.0 and 4.8 V (vs Li/Li^+) at RT. (a) Variation in discharge capacity (solid symbol) and midpoint potential (open symbol) vs cycle number. The midpoint potential is denoted as the potential when discharged to 50% of the cathode capacity. (b) Variation in energy density vs cycle number. The energy density is calculated based on the discharge capacity and midpoint potential.

For all the PO_4^{3-}-doped samples, the discharge capacities are relatively stable during long cycling (**Fig. 6a**). More evidently, the LNCMO-$(PO_4)_{0.01}$ sample delivers a larger discharge capacity, while the LNCMO-$(PO_4)_{0.05}$ electrode presents excellent long stability in discharge capacity during long cycling. Interestingly, the moderate rebound in discharge capacity is visible for the LNCMO-$(PO_4)_{0.05}$ electrode during extended cycles since the 80th cycle with the lower charge-transfer resistance and diffusion impedance during cycling (**Fig. S4**), on the basis of the continuous electrochemical activation of Li_2MnO_3-like components.[38-39] In respect to the discharge process, such plateau split in high and low potentials for the as-prepared sample are not observed for the PO_4^{3-}-doped samples with high PO_4^{3-} polyanion concentration (PO_4^{3-}=0.03 and 0.05) during long cycling, although the discharge midpoint potential is still observed to

decrease slightly. Differently, the discharge midpoint potential declines more slowly for the PO_4^{3-}-doped samples as compared to the as-prepared oxide. The high PO_4^{3-} polyanion concentration in the oxide is beneficial to stabilize the discharge midpoint potential as shown in **Fig. 6a**. Specifically, good energy density retention during long cycling, integrated with the discharge capacity and midpoint potential, further highlights the advantage of the PO_4^{3-} polyanion doping into the Li-rich layered oxide as presented in **Fig. 6b**. The energy density of the as-prepared oxide is higher for the initial 5 cycles, but sharper decline of the energy density can be clearly observed, attributed to both the fast discharge capacity degradation and evident midpoint potential decay. On the contrary, the PO_4^{3-}-doped oxides offer a relatively stable energy density during cycling. Thus, the LNCMO-$(PO_4)_{0.05}$ electrode presents excellent energy density retention during long cycling. Actually, the rebound in discharge capacity here can compensate the slow potential decay in order to maintain the stable energy density during long cycling.

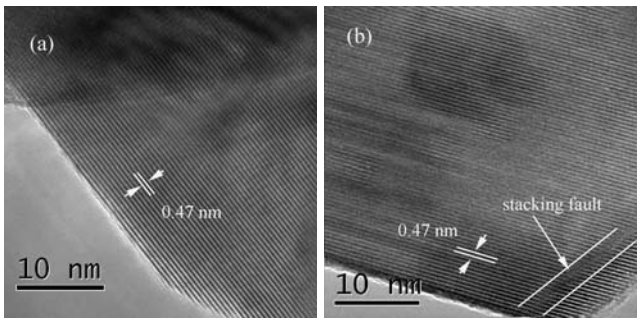

Fig. 7 TEM image of the oxides before cycling. (a) the as-prepared oxide. (b) the LNCMO-$(PO_4^{3-})_{0.05}$ oxide.

The undesirable discharge potential decay and plateau split are mainly related to the local structure change of the Li-rich layered oxides during cycling. It can be seen from TEM images (**Fig. 7**) that the pristine oxide shows perfect crystalline lattices, while a few lattice distortions (stacking fault) coexist with crystalline lattices in the LNCMO-$(PO_4)_{0.05}$ oxide due to the slight altering of the local environment by doping large tetrahedral PO_4^{3-} polyanions. The structure refinement is also conducted to provide the atomic parameters, as shown in Table S1-S3,[40] in which $Li_{1.17}Ni_{0.20}Mn_{0.58}Co_{0.05}O_2$ can be considered as 5/6 ($0.4Li_2MnO_3 \cdot 0.6LiNi_{0.4}Co_{0.1}Mn_{0.5}O_2$). As shown in **Fig. S5**, the differences between the calculated and observed curves are minimal, indicating the reliability of the refinement results. More specifically, Ni in Li layer decreases from 14.4% to 1.2% after doping PO_4^{3-} polyanions (Table S3). Such slight altering of the local environment is beneficial to stabilize the cycle life during long cycling. For the as-prepared oxide after 180 cycles (**Fig. 8**), the local spinel domains and amorphous domains are formed, in coexistence with the layered structure as a result of the release of oxygen and lithium in the form of Li_2O, and the subsequent migration of transition metal cations into Li sites. The local interlayer distance is slightly enlarged ($d \approx 0.48$ nm) due to the electrostatic repulsion between the oxygen layers under the lithium deficiency in the layered structure.[15] The appearance of the dominant spinel phase is in line with the widening of the low discharge potential plateau for the as-prepared oxide after 180 cycles (**Fig. 4**). In the case of the LNCMO-$(PO_4)_{0.05}$ oxide after 300 cycles, the lattice distortions (edge dislocation and stacking fault) and disordered (amorphous) domains can be found. Locally, the slight increase in interference fringe spacing can be also identified. It means in this work that high PO_4^{3-} polyanion concentration is beneficial to remain the parent layered structure and stable energy density of the PO_4^{3-}-doped oxides, although the local lattice distortions occur unavoidably after long cycling. As demonstrated previously, the surface modification with a layer thickness of 5–10 nm of Li-Mn-PO_4 or $FePO_4$ phosphate nanopartices is beneficial for the stability of the capacity during cycling.[22, 41] However, the potential decay is more serious due to the interface interaction (**Fig. S6**), leading to the inescapable decrease of energy density during cycling. It implies that the surface modification with phosphate nanopartices is not enough for stabilizing the energy density during long cycling. The surface modification with phosphate nanopartices and doping with PO_4^{3-} polyanions have the distinct effect on the electrochemical performance of the Li-rich layered oxides. In addition, the uniform distribution of phosphor in the LNCMO-$(PO_4)_{0.05}$ oxide is further demonstrated by the local chemical analysis with STEM-EDX (Figure S7). The phosphor-rich on the edge of the surface is not observed, confirming the absence of phosphate nanopartices on the surface of the LNCMO-$(PO_4)_{0.05}$ oxide. Of course, the peak intensity of phosphor is weak due to the trace presence of phosphor inside the oxide. Therefore, the effect of the surface modification with phosphates for the LNCMO-$(PO_4)_{0.05}$ oxide is eliminated based on the elemental distribution and electrochemical performance.

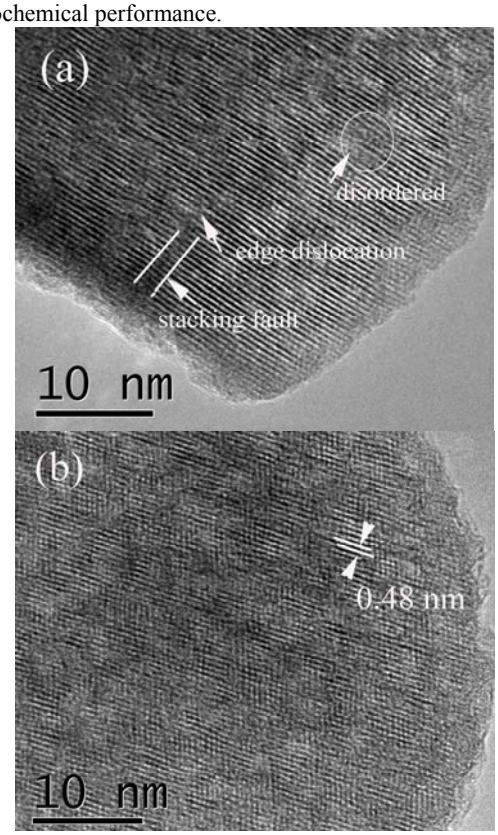

Fig. 8 TEM images of the oxides after long cycles at 0.1C rate. (a) the LNCMO-$(PO_4^{3-})_{0.05}$ oxide after 300 cycles. (b) the as-prepared oxide after 180 cycles.

The $LiMO_2$ and Li_2MnO_3-like component (M=Mn, Co and Ni)

are alternately arranged to form a layered structure with the stacking sequence of M/O/Li/O in the Li-rich layered oxide. Ni partially enters Li sites in the Li-layer, and Co coexists with Mn and residual Ni in the Li-M layer in the layered structure.[38] Apparently, the formation of the Li_2MnO_3-like component is of highly significance as the excess lithium reservoir and the framework for stabilizing $LiMO_2$ in the integrated layered structure.[42-44] The flexibility of the integrated layered structure is able to accommodate large variation in structure under high pressure–high temperature, including the derivation of more Li_2MnO_3-like components.[43] For example, large Na ions in the interlayer can adjust the activation extent of the Li_2MnO_3 component to improve the electrochemical performance.[45] After introducing PO_4^{3-} polyanions, large tetrahedral PO_4^{3-} polyanions with higher electronegativity in respect to spherical O^{2-} anions can alter the local environment of the Li-rich layered oxides moderately, which is more likely to be ascribed as a pillar effect (as shown in **Fig. 9**). The formation of Li_2MnO_3-like components is mainly attributed to the local strain by introducing large tetrahedral PO_4^{3-} polyanions. In particular, the fixing of Ni in the layered structure become stronger by PO_4^{3-} polyanion doping, as shown in XPS analysis and structure refinement (Table S1-S3). Usually, the cation ordering is highly related to the preparation condition and surface modification of Li-rich layered oxides, as well as the proton content in the lattice.[12-13, 46-47] In our case, PO_4^{3-} polyanion doping has a great impact on the cation ordering, where the Ni content in Li layer decreases obviously from 14.4% to 1.2% due to the stronger fixing of Ni by PO_4^{3-} polyanions in the layered structure. Correspondingly, the PO_4^{3-}-doped oxides presents the improved electrochemical performance during long cycling as compared with the as-prepared oxide, including both the discharge capacity and midpoint potential. It is noted that both the potential decay/plateau split and capacity degradation are sensitive to the local structure change of the Li-rich layered oxides, due to the migration of transition metal cations (Ni especially) into Li sites during long cycling, which can trigger the formation of spinel domains and break layered lattices in the layered structure.[36-37] As result, the lower Ni content in Li layer for the PO_4^{3-} polyanion doped sample can stabilize the layered structure. In addition, as the $LiMO_2$ and Li_2MnO_3-like component are alternately arranged, the structure change in any components may damage the integrated layered structure of the Li-rich layered oxide. Doping with PO_4^{3-} polyanions not only can stabilize the layered structure for the $LiMO_2$ component, but also can delay the subsequent structure change and insure the electrochemical activity of the Li_2MnO_3-like component, resulting in the continuous electrochemical activation as shown in **Fig. 6**. Therefore, the synergistic function of PO_4^{3-} polyanions in the oxide is apparent. Especially, when doped with high PO_4^{3-} polyanion concentration, the parent layered structure remains apparently with local lattice distortions during long cycling, due to the stronger anion bonding of PO_4^{3-} polyanions to transition metal cations (Ni especially) in the Li-rich layered oxides. Such imperfect layered structure is still important to maintain the stable energy density of Li-rich layered oxides. Meanwhile, the formation of spinel domains within the layered structure could be confined based on blocking transition metal cations into Li sites.

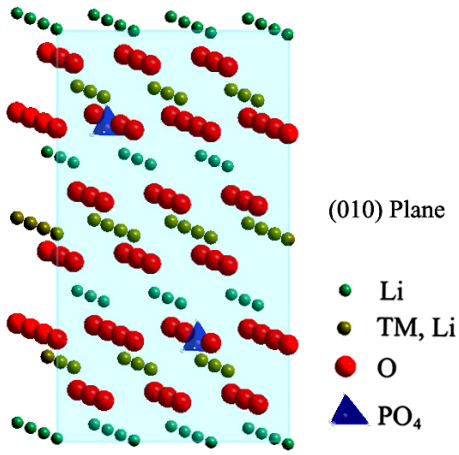

Fig. 9 The scheme of the PO_4^{3-}-doped layered structure.

4. Conclusions

In summary, in order to minimize the local structure change during long cycling, large tetrahedral PO_4^{3-} polyanions are introduced into the Li-rich layered oxide. As expected, the PO_4^{3-}-doped oxides presents the improved electrochemical performance during long cycling. In particular, the Li-rich layered oxide with the high PO_4^{3-} polyanion concentration provides relatively stable energy density during long cycling, due to the moderate local environment change in the oxide. Therefore, polyanion-doping offers a new route to fix transition metal cations in the parent layered structure, and thus stabilize energy density of the Li-rich layered oxides as cathode for high energy lithium ion battery.

Acknowledgements

Financial Supports from the NSFC (51072083), Research Fund for the Doctoral Program of Higher Education (20120031130002) and MOE Innovation Team (IRT13022) of China are gratefully acknowledged. The authors also wish to express their sincere thanks to Dr Xiaofei Bie and Prof. Yingjin Wei from Jilin University for the help in Reitveld refinement.

Notes and references

Institute of New Energy Material Chemistry, Collaborative Innovation Center of Chemical Science and Engineering (Tianjin), Tianjin Key Laboratory of Metal and Molecule Based Material Chemistry, Nankai University, Tianjin 300071, China. Fax: +86-22-23500876; Tel: +86-22-23500876; E-mail: xpgao@nankai.edu.cn

1 J. M. Tarascon, M. Armand, *Nature* 2001, **414**, 359.
2 X. P. Gao, H. X. Yang, *Energy Environ. Sci.* 2010, **3**, 174.
3 J. S. Lee, S. T. Kim, R. Cao, N. S. Choi, M. Liu, K. T. Lee, J. Cho, *Adv. Energy Mater*. 2011, **1**, 34.
4 Z. H. Lu, J. R. Dahn, *J. Electrochem. Soc*. 2002, **149**, A815.
5 M. M. Thackeray, C. S. Johnson, J. T. Vaughey, N. Li, S. A. Hackney, *J. Mater. Chem*. 2005, **15**, 2257.
6 A. R. Armstrong, M. Holzapfel, P. Novak, C. S. Johnson, S. H. Kang, M. M. Thackeray, P. G. Bruce, *J. Am. Chem. Soc*. 2006, **128**, 8694.
7 M. M. Thackeray, S. H. Kang, C. S. Johnson, J. T. Vaughey, R. Benedek, S. A. Hackney, *J. Mater. Chem*. 2007, **17**, 3112.

8 G. Z. Wei, X. Lu, F. S. Ke, L. Huang, J. T. Li, Z. X. Wang, Z. Y. Zhou, S. G. Sun, *Adv. Mater.* 2010, **22**, 4364.

9 N. Yabuuchi, K. Yoshii, S. T. Myung, I. Nakai, S. Komaba, *J. Am. Chem. Soc*. 2011, **133**, 4404.

10 J. Li, R. Klopsch, M. C. Stan, S. Nowak, M. Kunze, M. Winter, S. Passerini, *J. Power Sources* 2011, **196**, 4821.

11 T. Ohzuku, M. Nagayama, K. Tsuji, K. Ariyoshi, *J. Mater. Chem.* 2011, **21**, 10179.

12 W. He, J. F. Qian, Y. L. Cao, X. P. Ai, H. X. Yang, *RSC Advances* 2012, **2**, 3423.

13 H. Z. Zhang, Q. Q. Qiao, G. R. Li, S. H. Ye, X. P. Gao, *J. Mater. Chem*. 2012, **22**, 13104.

14 Y. K. Sun, M. J. Lee, C. S. Yoon, J. Hassoun, K. Amine, B. Scrosati, *Adv. Mater*. 2012, **24**, 1192.

15 D. Mohanty, S. Kalnaus, R. A. Meisner, K. J. Rhodes, J. L. Li, E. A. Payzant, D. L. Wood III, C. Daniel, *J. Power Sources*, 2013, **229**, 239.

16 Q. Y. Wang, J. Liu, A. V. Murugan, A. Manthiram, *J. Mater. Chem.* 2009, **19**, 4965.

17 J. Liu, A. Manthiram, *J. Mater. Chem*. 2010, **20**, 3961.

18 J. M. Zheng, Z. R. Zhang, X. B. Wu, Z. X. Dong, Z. Zhu, Y. Yang, *J. Electrochem. Soc.* 2008, **155**, A775.

19 H. Deng, I. Belharouak, C. S. Yoon, Y. K. Sun, K. Amine, *J. Electrochem. Soc.* 2010, **157**, A1035.

20 K. J. Rosina, M. Jiang, D. L. Zeng, E. Salager, A. S. Best, C. P. Grey, *J. Mater. Chem*. 2012, **22**, 20602.

21 D. Shin, C. Wolverton, J. R. Croy, M. Balasubramanian, S. H. Kang, C. M. Lopez Rivera, M. M. Thackeray, *J. Electrochem. Soc*. 2012, **159**, A121.

22 Q. Q. Qiao, H. Z. Zhang, G. R. Li, S. H. Ye, C. W. Wang, X. P. Gao, *J. Mater. Chem*. A, 2013, **1**, 5262.

23 Y. H. Wang, X. Yan, X. F. Bie, Q. Fu, F. Du, G. Chen, C. Z. Wang, Y. J. Wei, *Electrochim. Acta* 2014, **116**, 250.

24 Y. S. Meng, G. Ceder, C. P. Grey, W. S. Yoon, M. Jiang, J. Breger, Y. Shao-Horn, *Chem. Mater.* 2005, **17**, 2386.

25 A. Boulineau, L. Croguennec, C. Delmas, F. Weill, *Chem. Mater.* 2009, **21**, 4216.

26 http://www.wiredchemist.com/chemistry/data/atomic-and-ionic-radii.

27 W. He, D. D. Yuan, J. F. Qian, X. P. Ai, H. X. Yang, Y. L. Cao, *J. Mater.Chem*. A 2013, **1**, 9760.

28 N. Li, R. An, Y. F. Su, F. Wu, L. Y. Bao, L. Chen, Y. Zheng, H. F. Shou, S. Chen, *J. Mater.Chem*. A 2013, **1**, 9760.

29 K. M. Shaju, G. V. S. Rao, B. V. R. Chowdari, *Electrochim. Acta* 2002, **48**, 145.

30 C. Nithya, V. S. S. Kumari, S. Gopukumar, *Phys. Chem. Chem. Phys*. 2011, **13**, 6125.

31 P. R. Kumar, M. Venkateswarlu, M. Misra, A. K. Mohanty, N. Satyanarayana, *J. Electrochem. Soc*. 2011, **158**, A227.

32 B. N. Hu, X. Y. Wang, H. B. Shu, X. K. Yang, L. Liu, Y. F. Song, Q. L. Wei, H. Hu, H. Wu, L. L. Jiang, X. Liu, *Electrochim. Acta* 2013, **102**, 8.

33 E. Markevich, R. Sharabi, H. Gottlieb, V. Borgel, K. Fridman, G. Salitra, D. Aurbach, G. Semrau, M.A. Schmidt, N. Schall, C. Bruenig, *Electrochem.Commun*. **2012**, 15, 22.

34 C. V. Ramana, A. Ait-Salah, S. Utsunomiya, J. F. Morhange, A. Mauger, F. Gendron, C. M. Julien, *J. Phys. Chem. C*, **2007**, 111, 1049.

35 E. Etienne, F. Cavani, R. Mezzogori, F. Trifiro, G. Calestani, L. Gengembred, M. Guelton, *Appl. Catal. A* 2003, **256**, 275.

36 M. Gu, I. Belharouak, J. M. Zheng, H. M. Wu, J. Xiao, A. Genc, K. Amine, S. Thevuthasan, D. R. Baer, J. G. Zhang, N. D. Browning, J. Liu, C. M. Wang, *ACS Nano* 2013, **7**, 760.

37 B. Xu, C. R. Fell, M. Chi, Y. S. Meng, *Energy Environ. Sci*. 2011, **4**, 2223.

38 C. S. Johnson, N. C. Li, C. Lefief, J. T. Vaughey, M. M. Thackeray, *Chem. Mater*. 2008, **20**, 6095.

39 S. H. Yu, T. Yoon, J. Mun, S. Park, Y. S. Kang, J. H. Park, S. M. Oh, Y. E. Sung, *J. Mater. Chem. A* 2013**, 1**, 2833.

40 M. Morishita, T. Mukai, T. Sakamoto, M. Yanagida, T. Sakai, *J. Electrochem. Soc*. 2013, **160**, A1311.

41 Z. Y. Wang, E. Z. Liu, C. N. He, C. S. Shi, J. J. Li, N. Q. Zhao, *J. Power Sources* 2013, **236**, 25.

42 S. Kim, C. Kim, J. K. Noh, S. Yu, S. J. Kim, W. Chang, W. C. Choi, K. Y. Chung, B. W. Cho, *J. Power Sources* 2012, **220**, 422.

43 C. R. Fell, D. H. Lee, Y. S. Meng, J. M. Gallardo-Amores, E. Moran, M. E. Arroyo-de Dompablo, *Energy Environ. Sci*. 2012, **5**, 6214.

44 F. Amalraj, D. Kovacheva, M. Talianker, L. Zeiri, J. Grinblat, N. Leifer, G. Goobes, B. Markovsky, D. Aurbach, *J. Electrochem. Soc.* 2010, **157**, A1121.

45 B. Qiu, J. Wang, Y. G. Xia, Y. Z. Liu, L. F. Qin, X. Y. Yao, Z. P. Liu, *J. Power Sources* 2013, **240**, 530.

46 T. A. Arunkumar, E. Alvarez, A. Manthiram, *J. Mater. Chem*. 2008, **18**, 190.

47 D. Mohanty, A. S. Sefat, S. Kalnaus, J. L. Li, R. A. Meisner, E. A. Payzant, D. P. Abraham, D. L. Wood, C. Daniel, *J. Mater. Chem. A* 2013**, 1**, 6249.